Title: Fabrication and Characterization of a Submillimeter-Scale Ultrasonic Motor

Author: Kohei Kikuchi, Mudassir Hussain, and Tomoaki Mashimo*

* Corresponding author:

Okayama University

3-1-1 Tsuchimanaka, Kitaku, Okayama, 700-8530, Japan

mashimo @ okayama-u.ac.jp

Abstract

Submillimeter-scale electrically driven micromotors have the potential to revolutionize micro-robotic systems, but difficulties in their fabrication processes and unknown physical phenomena prevent their development. In this paper, we propose a submillimeter-scale rotary piezoelectric ultrasonic motor with the smallest stator (0.41 mm × 0.41 mm × 0.25 mm) reported to date. The micromachining technologies enable the creation of tiny components. A micromanipulator that can control a small amount of adhesive of sub-milligram order engenders success in manufacture of the stator. Several experiments clarify the submillimeter-scale physical behaviors, such as the admittance and the quality factor. With appropriate piezoelectric materials, submillimeter-scale ultrasonic motors are built and characterized using a rotor with 0.15 mm diameter. The motor with typical hard PZTs demonstrated maximum torque of 5.4 nNm and a maximum angular velocity of 714 rad/s at an applied voltage with amplitude of 44.8 $V_{p\text{-}p}$. Furthermore, another motor with single-crystal PMN-PT piezoelectric elements presented the possibility of low-voltage actuation. These submillimeter-scale ultrasonic motors were compared with existing comparable-size micromotors.

1 Introduction

Micromotors are of great interest as key components to create new micro-robotic systems such as micro-fluidic systems, minimally invasive medical devices, and insect-scale rescue robots. Biological machines with a new type of microactuator might offer unprecedented motions and functions that small creatures can achieve in nature. Various principles and methodologies have been proposed and developed since the 1980s to realize micromotors [1]. Their main principles can be classified into three types [2,3]: electromagnetics, electrostatics, and piezoelectricity. Electromagnetic motors are the most commonly used actuators, but their miniaturization to the submillimeter scale encounters difficulties for fabrication because of their complicated components [4,5]. Furthermore, severe torque dissipation attributable to the physics of scaling loses practicality [6, 7]. Electrostatic motors, which have a better scaling law [8–10], can be fabricated using micro-electromechanical systems (MEMS) technologies, but their low output torque restricts further deployment.

Piezoelectric ultrasonic motors are anticipated as promising micromotors because they have two important features that are necessary for miniaturization into millimeter or submillimeter scales. The first feature is that piezoelectric elements and actuators can generate a certain strain no matter how small they are. Even at submillimeter-scale or smaller, the applied voltage can be converted to displacement and force. Another feature is their simple structure, which comprises only a few components. Piezoelectric elements and ceramics can be fabricated using common fabrication procedures such as sintering and dicing without using complex silicon-based processes.

During the past two decades, many researchers have studied the miniaturization of ultrasonic motors [11–13]. Most miniature ultrasonic motors have used a bending vibration mode as their principle [14–16]. It is effective for long cylindrical stators (e.g., 1.5 mm diameter and 5 mm length) to enlarge the vibration amplitude, but the short length sharply reduces the amplitude and results in a decrease in output. Recently, the study of the miniaturization of ultrasonic motors has reached a 1–2 mm scale. One of the smallest ultrasonic motors uses a cylindrical stator with 0.25 mm diameter and 1 mm length. It couples axial and torsional modes in a helically cut stator [17, 18]. The total length including piezoelectric elements becomes 1.5 mm. Another tiny ultrasonic motor uses shear modes generated in a rectangular PZT-bulk element with 1.55 mm length [19].

We have also studied the miniaturization of ultrasonic motors. Our approach is the use of a vibration mode that produces a travelling wave with three waves inside the hole of the stator circumferentially [20]. The advantage of using this circumferential travelling wave is that the stator can generate a certain torque even at the cube or flat, unlike the bending mode, which decreases the torque at a short length. In fact, one of our reports describes that the performance of using the three-waves is better than the bending mode when the length is short [21]. For example, one prototype stator measures 1.6 mm $\times$ 1.6 mm $\times$ 1 mm and can generate a torque of 40 μNm, which is the greatest torque in the similar-scale ultrasonic motors [22]. These results represent the possibility of further miniaturization using the three-wave mode. How small it can become is of great interest in the realm of microengineering.

In this paper, we propose a submillimeter-scale traveling wave ultrasonic motor using a 0.41 mm $\times$ 0.41 mm $\times$ 0.25 mm stator, which is the smallest rotary ultrasonic motor reported to date. This size is comparable to an early MEMS-based electrostatic micromotor [8], except for the thickness that the silicon-based fabrication cannot increase. Reducing the stator size to submillimeter scale encounters not only difficulties in fabrication but also of underlying physical phenomena, such as changes in damping. We examine these difficulties to achieve the submillimeter-scale ultrasonic motors and clarify through experiments how the physics of scaling behaves with miniaturization.

The main contributions of this paper are summarized as follows:

1. The smallest ultrasonic motor, with size comparable to those of the silicon-based micromotors, is built and demonstrated. Although its performance is still under development, this smallest motor can be a fundamental technology for microrobots that can accomplish innovative tasks.

2. Proposed fabrication and manipulation techniques for the smallest motor are based on common machining processes used in macroscale. Therefore, engineers can start the construction of similar-sized components cost-effectively for the creation of microrobots.

In the remainder of the paper, we describe the basic models in section II. Section III explains the fabrication of components and the adhesion method for the stator. The selection of materials for the tiny stator, such as PZT materials, is discussed in Section IV. Section V demonstrates the generation of a rotary motion and analyze

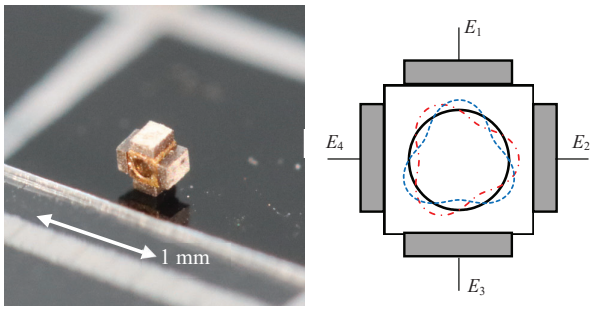

(a) (b)

Fig. 1. (a) Stator for submillimeter-scale ultrasonic motor. (b) Three-wave mode used for generating a rotation: the first three-wave mode (dotted line) generated by voltages E_1 and E_3, and the second three-wave mode (dashed line) generated by voltages E_2 and E_4.

dynamic characteristics.

2 Principle of the Stator

2.1 Fundamental Principle

The principle of the proposed submillimeter-scale ultrasonic motor must be described briefly. Related details are explained in an earlier report [20]. The prototype stator comprises a tiny metallic cube with a hole and four PZT elements adhered to the side surfaces of the cube, as shown in Fig. 1(a). The stator excites a vibration mode that generates three waves along the circumference of the center hole. As shown in Fig. 1(b), when voltages $E_1 = A_E \sin 2\pi f_E t$ and $E_3 = -A_E \sin 2\pi f_E t$ are applied to the upper and lower PZT elements, respectively, they repeat expansion and contraction, exciting the three-wave mode (dotted line in Fig. 1(b)). For these voltages, A_E and f_E denote the amplitude and frequency, respectively. Also, f_E is adjusted to the natural frequency of the stator. Similarly, when applying $E_2 = A_E \cos 2\pi f_E t$ and $E_4 = -A_E \cos 2\pi f_E t$ to the left and right elements, the stator excites another three-wave mode (dashed line) with a temporal phase difference of $\pi/2$. When the two three-wave modes are excited simultaneously, a traveling wave is generated around the hole circumference. This travelling wave generates an elliptical motion that transfers the driving force to the rotor.

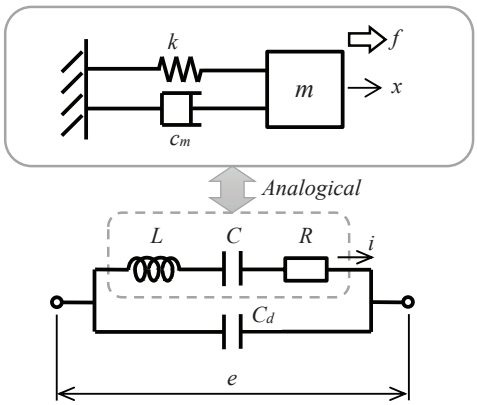

Fig. 2. Electric and mechanical model of ultrasonic motors: this model can be applied to the submillimeter-scale ultrasonic motor.

2.2 Physics with Miniaturization

This subsection clarifies how the electric and mechanical characteristics behave with miniaturization. In piezoelectric actuators having electrical and mechanical models in a single solid, the equation of motion can be expressed in the same form as the differential equation of the equivalent circuit. As with the piezoelectric actuators, the ultrasonic motors are also described by the differential equations of electromechanical coupling.

The stator vibration can be formulated as described hereinafter. The electric model comprises inductance L, capacitance C, resistance R, and damped capacitance C_d, as shown in Fig. 2. Voltage e is applied in the circuit, and current i flows at the LCR serial part. Some of the electric energy is stored and consumed in the LCR serial circuit. The remainder of the energy is stored in the damped capacitance. The energy supplied to the LCR serial circuit is equal to the mechanical energy consumed in the actuator part. We express the relation as an equivalent circuit that can estimate the mechanical vibration. With voltage $e = E_i \cos \omega t$ applied to the LCR serial circuit, the relation between the voltage and current is expressed using a differential equation as

$$L\frac{di}{dt} + Ri + \frac{1}{C}\int idt = E_i \cos \omega t \tag{1}$$

where E_i and ω are the amplitude and the frequency of the applied voltage, respectively. Fig. 2 shows the mechanical system with a mass, a damper, and a spring. When a periodic force $f = F_i \cos \omega t$ acts on the mass in the mechanical model, the equation of motion is

$$m\ddot{x} + c_m\dot{x} + kx = F_i \cos \omega t \tag{2}$$

where F_i and ω are the amplitude and frequency of the external force, respectively. Also, ω takes the same value as that in (1). Consequently, the electrical and mechanical models described by the same form exist in the stator of an ultrasonic motor. In other words, by measuring the electric characteristics of the stator, the mechanical characteristics can be estimated.

We can examine the behavior of the electromechanical parameters of the stator with miniaturization. Table 1 shows that the parameters in the electromechanical models are scaled by a length parameter l [23]. Here, the scale of the resonant resistance R is defined to correspond to an actual behavior where R increases with downscaling. Theoretically, the resonant resistance is scale-invariant in the macro scale. The increase in the resonant resistance with miniaturization affects the damping of the mechanical system. Although the viscous friction coefficient c varies with the area ($c \propto l^2$) in the normal equation of motion, its scale become l^3 with damping corresponding to the behavior of the resonant resistance.

The relation described above suggests the scale of the resonance frequency of the electrical system and the natural frequency of the mechanical system:

$$\omega_r = \frac{1}{\sqrt{LC}} = \sqrt{\frac{k}{m}} \propto l^{-1} \tag{3}$$

An interesting point is that the mechanical natural frequency takes the same value as the electrical resonance frequency in an electromechanical system. First, the natural frequency is determined mechanically from material parameters and the stator design. Electric parameters L and C are followed to correspond with the natural frequency. To excite a harmonic vibration for enlarging the vibration amplitude of the piezoelectric actuator, voltage frequency ω in (1) is set to natural frequency ω_r

A quality factor is an important parameter indicating the sharpness of the resonance. A quality factor is known as a material parameter Q_m of piezoelectric ceramics determined at a standard shape, e.g., a circular plate with 10 mm diameter and 1 mm thickness [24]. Given high Q_m, a current flows with high efficiency because of low dissipation. We evaluate the quality factor of submillimeter-scale ultrasonic motor in later

Table 1: Scale of the physical magnitudes of piezoelectric actuators

Quantity		Scale
Inductance	L	l^1
Resonant resistance	R	l^{-1}
Capacitance	C	l^1
Damping capacitance	C_d	l^1
Mass	m	l^3
Damping coefficient	c_m	l^1
Spring coefficient	k	l^1

experiments. Scaling of Q_m is obtained from the electromechanical parameters:

$$Q_m = \frac{\omega_r L}{R} = \frac{\sqrt{mk}}{c_m} \propto l^1 \tag{4}$$

Quality factor Q_m of the stator increases with size, although the normal quality factor in macro scale is scale-invariant. The scale of the quality factor and the resonant resistance is detailed in Appendix.

2.3 Modeling of the Rotational Motion

The stator vibration transfers to the rotor inserted into the stator hole via friction. The dynamic behavior of the motor is evaluated to analyze the output characteristics, such as the angular velocity and torque. When the motor generates constant torque τ, a rotor with a moment of inertia J spins with an angular velocity ω. The equation of motion of the rotor is expressed as a first-order system as

$$J\dot{\omega} + \xi\omega = \tau \tag{5}$$

where ξ is the viscous friction coefficient determined by the vibration velocity of the stator in experiments. The extent of its vibration corresponds to the magnitude of the current in (1) and velocity in (2). In other words, a design with a higher admittance (or lower impedance) increases the vibration speed, leading to a higher angular velocity of the rotor.

3 Stator Prototype

3.1 Fabrication of the Components

Miniaturization of the piezoelectric micromotors generally involves novel challenges with complicated fabrication techniques such as a hydrothermal method [14], laser micro- machining [17], and silicon-based fabrication [25] [26]. Making such new technologies is undoubtedly beneficial, but it is too time-consuming and cost-intensive to stabilize manufacturing. We employ conventional micromachining to fabricate the submillimeter-scale components to realize the smallest ultrasonic motor. Fig. 3(a) shows the stator components: a metallic cube and piezoelectric elements. Their fabrication can be explained as follows.

Fig. 3(b) illustrates the metallic cube fabrication process. First, a square prism with a base of 0.25 mm $\times$ 0.25 mm is machined from the base material of phosphor bronze. After being fixed using solid wax that is often used for micromachining, the square prism is formed into a cube. Finally, a 0.15 mm diameter hole is opened at the center of the cube fixed to a jig. The hole diameter is comparable to the smallest silicon-based micromotors [8]. In the resultant stator shown in Fig. 3(a), the maximum error between side a and side b is within 4 μm. The error of side c has little relation to the motor performance.

Piezoelectric elements measure a surface of 0.25 mm $\times$ 0.20 mm and 80 μm thickness and can also be fabricated by regular processes. After sintering in a high-temperature oven, the surfaces of the thin plate piezoelectric material are coated by the electrodes using sputter deposition. Here, sputter deposition is preferred rather than silver-sintered electrodes because of its better damping characteristics. After polarization, the piezoelectric elements are cut from the thin plate using a dicing saw. To distinguish the polarization direction, one surface has a silver electrode. The other surface has a bronze electrode (Fig. 3(a)). In section IV, we present investigation of several piezoelectric materials under the constant piezoelectric element dimensions.

3.2 Micromanipulation for Adhesions

Building the stator of the submillimeter-scale ultrasonic motor encounters difficulties of fabrication, such as the handling tiny parts and adhesion of components. Because the submillimeter-scale components are barely visible to the naked eye, all procedures are performed under microscopic environments. One of the most important

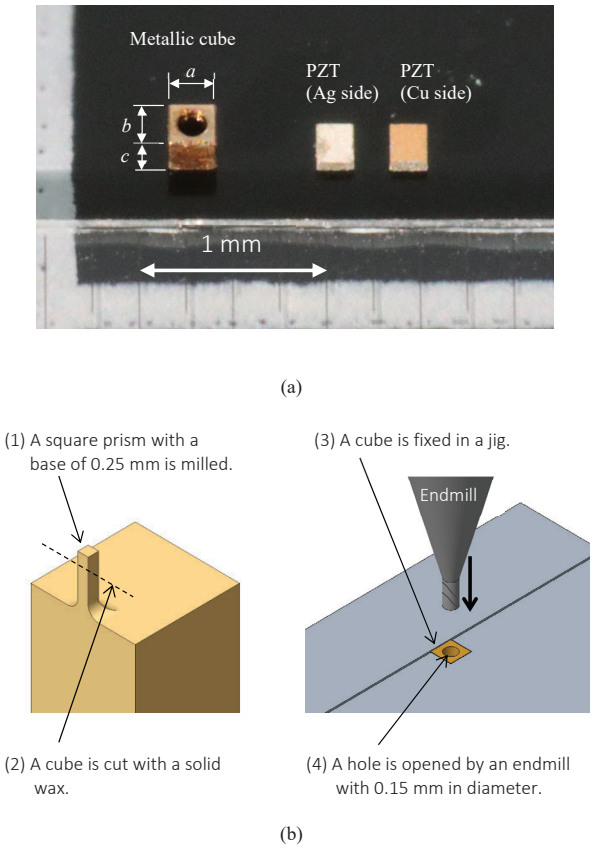

Fig. 3. (a) Components of the stator, and (b) the fabrication method for the metallic cube.

process is the glue adhesion process. The amount of glue adhering to one piezoelectric element is of microgram order. The amount of glue must be almost equal for each piezoelectric element to make the stator quality stable. At the submillimeter scale, a variation in the amount of glue causes a large change in motor performance.

To enable micro-adhesion between the metallic part and piezoelectric elements, we construct a micromanipulator to take a subtle amount of the adhesive, as shown in Fig. 4(a). The manipulator can be controlled with three-axis numerical control (NC) positioner. A needle with the finest tip of 0.1 mm is attached to the NC positioner. It can be controlled with a minimum step of approximately 10 μm. From the upper side of the conductive adhesive, the needle is moved slowly downward in the z-direction. The needle tip, which is connected to a continuity sensor, detects contact with the conductive adhesive. We designate this position as the original position ($z = 0$ mm). From this position, the amount of the adhesive increases with the amount of the dip (movement in the z-direction). In other words, the small displacement can make the needle tip take a small

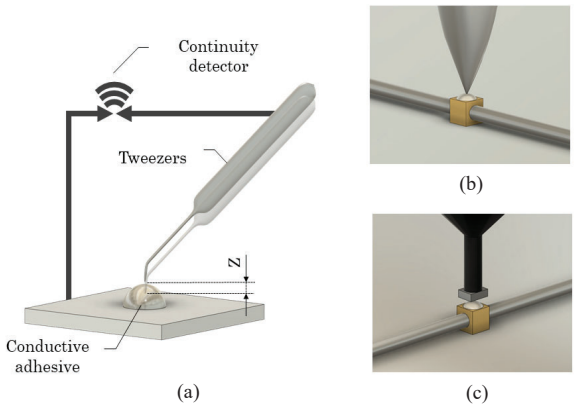

Fig. 4. Adhesion procedure using a micromanipulator controlled by a numerical control positioner: (a) an adhesive is taken by the tip of a tweezer, (b) the adhesive is placed on a surface of the metallic cube, and (c) a PZT attached to a vacuum tweezer is placed on the adhesive.

amount of adhesive, or vice versa.

The sample diameter and height can be estimated roughly using a microscope with image processing. The conductive adhesive (XA-874, Fujikura Kasei co., Tokyo, Japan) is used for bonding the metallic cube and the piezoelectric elements. Fig. 5(a) shows examples of the adhesive sampled by the micromanipulator. The adhesives are moved onto a plate five times. Also, five cases of different z-displacement are conducted. The smallest sample that the needle can manipulate has approximately 72 μm diameter. Fig. 5(b) summarizes the relation between the depth in the z direction and the adhesive diameter. From this relation, the optimal amount of the adhesive was obtained: The amount at a $z = 0.3$ mm depth was closest to the desired amount. Fig. 5(c) shows one sample at a depth of $z = 0.3$ mm. The adhesive diameter is approximately 139 μm. The height is about 46.9 μm.

The conductive adhesive at the needle tip is moved to the center of the metallic cube (Fig. 4(b)) by the NC positioner. During the adhesion process, a shaft has been inserted into the hole of the metallic cube to fix its position. When the system detects the contact between the metallic cube and the conductive adhesive on the needle, the needle is moved upward. After confirming the appropriate amount of the adhesive visually, the piezoelectric element is placed at the center of the metallic cube. For this process, the manipulator requires a tool for handling tiny piezoelectric elements. Adhesion forces and surface tension become dominant in the microdomain, unlike those in the gravity domain. The submillimeter components cannot be detached from tweezers because of the

surface tension force. To handle a submillimeter-scale piezoelectric element, we replaced the needle with a vacuum tweezer in the NC positioner. With the assistance of the microscope, the vacuum tweezer with the tiny piezoelectric element moves down until the piezoelectric element presses the cube (Fig. 4(c)). By repeating this process from adhesion to placement four times, the stator with four piezoelectric elements is completed.

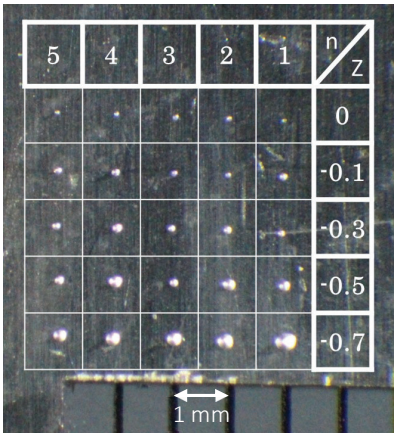

(a)

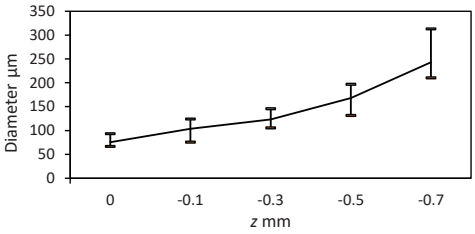

(b)

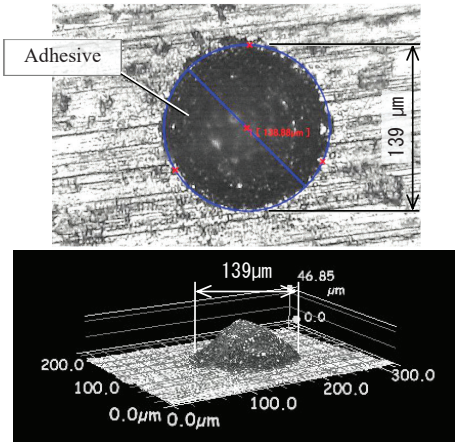

(c)

Fig. 5. (a) Samples of the adhesive: horizontal column shows trial times and vertical line mean the amount of the dip of the needle. (b) The relationship between the diameter of the adhesive and the dip amount of the needle. Error bars mean the maximum and minimum values. (c) An adhesive observed by the microscope with image processing when $z = 0.3$ mm. This amount is used for the adhesion of the piezoelectric elements.

Table 2: Material properties of piezoelectric elements

		Hard PZT	Soft PZT	PMN-PT
Coupling coefficient	k_{31}	0.32	0.36	-
	k_{33}	0.54	0.68	0.94
	k_{15}	0.50	0.57	-
Piezoelectric constant	d_{31}	-131	-303	-
($\times 10^{-12}$ m/V)	d_{33}	225	603	1800
	d_{15}	294	592	-
Quality factor	Q_m	2070	70	80
Curie Temp. (°C)	T_c	360	180	140
Coercive field (kV/mm)	E_c	-	-	0.22

Values obtained via standard measurements based on JEITA EM-4501 [24].

4 Evaluation of the Stator

Hard PZT materials with a high quality factor are commonly used for ordinary-sized ultrasonic motors because of their high efficiency. However, soft PZT materials can generate a larger vibration amplitude than hard materials because of a high piezoelectric constant, although they reduce energy efficiency. In this section, we examine what kinds of piezoelectric materials are suited for the submillimeter-scale ultrasonic motor.

Table 2 shows some characteristics of the three piezoelectric materials selected: a hard PZT, a soft PZT, and a single-crystal PMN-PT. Hard PZT materials have a high quality factor that reduces damping and heat generation and results in an increase in energy efficiency. Soft materials have low quality factor but show a higher piezoelectric constant than hard materials. A single crystal material, the characteristics of which are similar to the soft material, has the highest piezoelectric constants of the three materials. Recently, single-crystal PMN-PT is available [27], but the low coercive field limits the motor output. Furthermore, hard PZT elements with two polarization directions are evaluated: hard PZTs are polarized to expansion mode (31-mode) and thickness-shear mode (15-mode). In general, PZTs used for ultrasonic motors are 31-mode, but 15-mode have a higher piezoelectric constant and a higher coupling factor. The use of 15-mode has improved the quality factor and coupling coefficients of the stator, leading to higher energy efficiency [22]. The other materials, the soft PZT and single-crystal PMN-PT, are polarized to 31-mode. In total, four stators with hard PZT (31-mode) elements, hard PZT (15-mode) elements, soft PZT elements, and single-crystal PMN-PT elements are bonded to the tiny metallic cubes for the stator.

Modal analysis using finite element method (FEM) shows the mode shape and natural frequency of the three-wave mode. The dimensions and material parameters of the analytical stator model are ascertained from those of the prototype stator used for the experiments. Modal analysis of the stators with the four piezoelectric materials is conducted with a free boundary condition. The results obtained using FEM analysis show that the natural frequency of the three-wave mode increases at smaller sizes, as estimated in (3). The resonance frequency of the stators with four piezoelectric materials is approximately 4 MHz.

Measuring the frequency response of the admittance indicates the existence of resonance electrically. To obtain the electrical connection, the stator assembly is fixed inside an acrylic jig by spring contact probes. Fig. 6 shows the stator placed in the jig. The place the contact probes support is in the neighborhood of the antinodes of the three-wave mode. Ideally, the stator should be fixed at its nodes to avoid suppressing the stator vibration. However, holding designated points on the stator is difficult because it is too small to be held. At present, the use of the jig is the best method for placing the stator. For admittance measurements, a signal line and a ground line from an impedance analyzer (FRA5087; NF Corp., Japan) are connected to the top and bottom PZT elements, respectively. When the prototype stator resonates, a larger current flows due to the decrease in the impedance. These resonant frequencies show good agreement with estimation of the FEM piezoelectric analysis (Fig. 7).

Fig. 8 shows the frequency characteristics of the admittance of the prototype stators when the frequency is 3.6–4.8 MHz. The single-crystal PMN-PT shows the highest admittance at 4 MHz. The soft PZT (31-mode) is the second highest at 4.2 MHz in the four stators. In contrast, the stators using hard PZT materials show low admittance. Apparently, miniaturization to the submillimeter scale increases the damping and resonant resistance of the stator using hard PZTs. Particularly, the admittance of the hard PZT polarized to 15-mode is the smallest among the four. The most likely reason is that the dicing process along the polarization direction caused depolarization in the thickness-shear direction. Table 3 shows the quality factor and coupling coefficient of the stators, measured by the impedance analyzer. In these, the stator with hard PZT elements has a high quality factor. This value is close to one-third of the quality factor of the stator with a side length of 1 mm [22]. It roughly accords to the estimation in (4). The stator with PMN-PT elements shows the highest coupling factor which enables the actuation at low voltages.

Based on these findings, we selected a hard PZT (31-mode) as the most typical piezoelectric element and

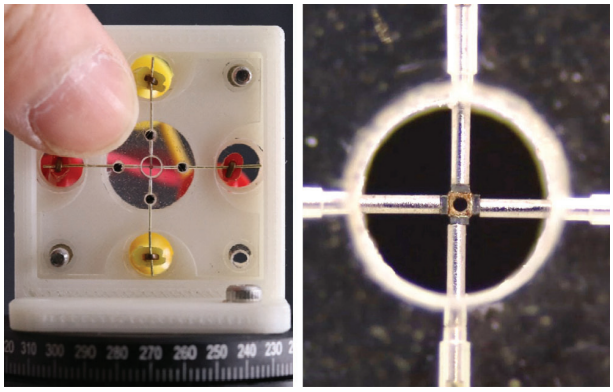

(a) (b)

Fig. 6. Stator installed at an acrylic jig: the stator is fixed by four contact probes that supply the input power. (a) detailed view of the stator and (b) the rotor and load.

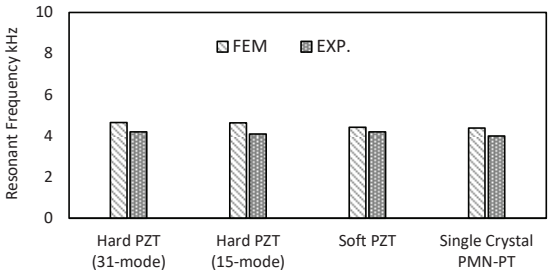

Fig. 7. Comparison between the FEM analysis and experiments.

selected the single-crystal material as the potential one. Motor performance with piezoelectric elements of two kinds is evaluated as described in the next section.

5 Motor Characterization

5.1 Experimental Setup

A two-channel wave generator (WF1974; NF Corp., Japan) and power amplifiers (BA4825; NF Corp., Japan) are used to generate voltages. The amplitude and frequency can be adjusted using the wave generator and amplifiers. To generate a voltage with a reversed phase, two transformers are used between the amplifiers and the stator. For example, when a voltage $E_1 = A_E \sin 2\pi f_E t$ is input to a transformer, a negative phase voltage $E_3 = -A_E \sin 2\pi f E_t$ is output from another terminal of the transformer. As with the sine phase, voltages $E_2 = A_E \cos 2\pi f_E t$ and $E_4 = -A_E \cos 2\pi f_E t$ are prepared. Then the voltages, E_1 to E_4, are applied through the

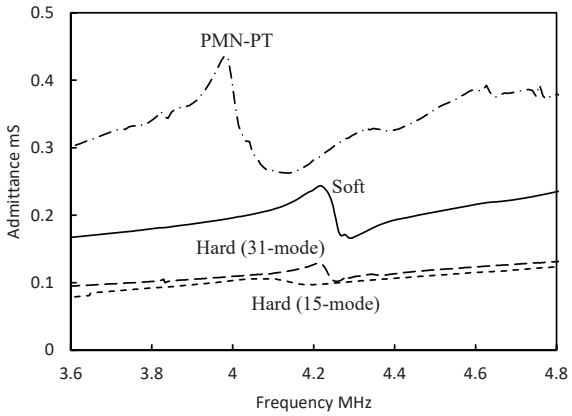

Fig. 8. Frequency characteristics of the admittance.

Table 3: Characteristics of prototype stators

	f_r MHz	Q_m	k_{33} %
Hard PZT (31-mode)	4.21	49.8	0.839
Hard PZT (15-mode)	4.10	7.18	1.22
Soft PZT	4.22	51.4	0.848
PMN-PT	3.99	15.5	3.41

f_r: Resonant frequency, Q_m: Quality factor, k_{33}: Coupling coefficient

contact probes in the same acrylic jig (Fig. 5). The contact probes play an important role not only in supplying electric power but also in maintaining the stator's position during rotary motion.

Fig. 9 shows components for characterizing the submillimeter ultrasonic motor. A rotor with a diameter of 0.150 mm and a length of 10 mm is inserted into the stator hole. The tapered shape at the rotor center prevents rotor movement in the axial direction. The inner diameter of the stator hole (0.152 mm) is slightly larger than the rotor diameter, providing a gap of a few micrometers between the stator and the rotor. This gap has been selected experimentally by adjusting the rotor diameters with a micrometer-order difference. A large gap increases the shake of the rotor during rotation. An overly small gap restricts the rotation because of an increase in friction. A weight with the moment of inertia $J = 8.2 \times 10^{-15}$ kgm^2 is attached to the end of the rotor because the angular acceleration is too high to be measured.

To evaluate the torque and angular velocity, the rotor motion is recorded using a high-speed camera (VW-

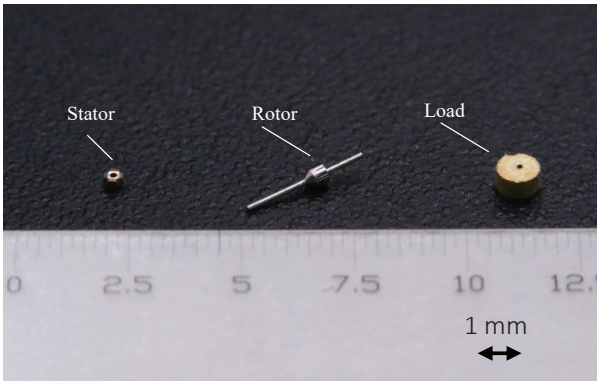

Fig. 9. Components for the submillimeter-scale ultrasonic motors. From left, the stator, rotor and a load.

9000; Keyence Co., Japan). A thin fin with a marker is attached to the end of the rotor to track the rotation. Time-history data of the angular displacement are accumulated by tracking the rotor movement in successive images recorded using a high-speed camera. Time derivation derives the angular velocity and angular acceleration of the rotor.

5.2 Characterization of the Submillimeter-Scale Motor

A high electric field depolarizes a piezoelectric material. The degree of depolarization depends on the grade of material, time, temperature, and other factors. An alternating current also has a depolarizing effect during each half cycle. Because of this depolarization, the piezoelectric elements become unable to produce strain for the motor torque. For example, a manufacturer of PZT ceramics has published the limit of an electric field applicable (coercive field) as high as 600 $\mathrm{V/mm}$ for DC and 320 $\mathrm{V/mm}$ for the AC field for a hard PZT material [28]. For 80 μm thickness, the maximum voltage must be less than 60 $\mathrm{V_{p-p}}$ for our submillimeter ultrasonic motor with hard PZTs. As with the hard PZT, the coercive field of the single-crystal PMN-PT is 80 $\mathrm{V/mm}$. The maximum voltages applied to that with the same thickness are about 15 $\mathrm{V_{p-p}}$. In experiments, voltages lower than the coercive field are applied to avoid the breakdown: voltages with amplitudes of 44.8 $\mathrm{V_{p-p}}$ and 11.8 $\mathrm{V_{p-p}}$ are applied to the stator with the hard-PZT and the single-crystal PMN-PT, respectively.

Micromotors with the hard PZT and the single-crystal PMN-PT are evaluated experimentally using the transient response. The amplitude of the voltages is adjusted so as not to be greater than the voltage corresponding to the coercive field of the material. Fig. 10(a) shows the transient response of the micromotor with the hard

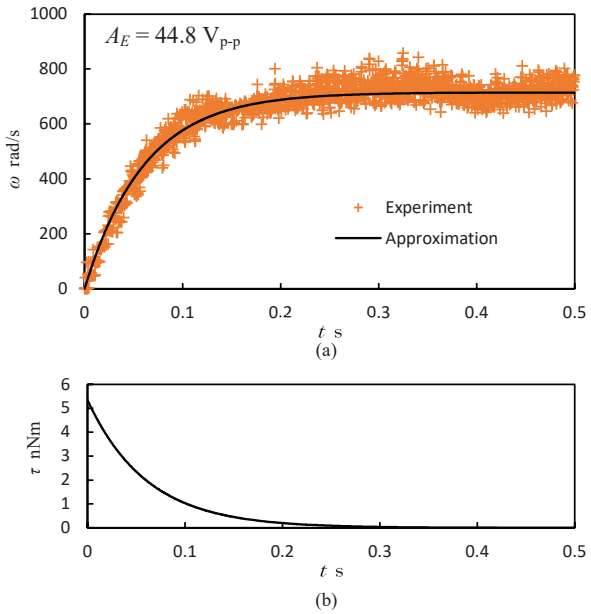

Fig. 10. Transient response of the micromotor using the stator with hard piezoelectric elements (31 mode). (a) Experimental plots and an approximation curve obtained from the least minimum method. (b) the torque obtained from the approximated angular velocity curve.

PZTs when a voltage with amplitude of 48.8 V_{p-p} is applied. After the rotor starts to spin, the angular velocity reaches a peak speed of $t = 0.2$ s. The experimentally obtained result involves noise during the rotation because of the stator–rotor interface conditions such as friction, gap, and surface roughness. The experimental plots are approximated to the first-order system given in (5) using least squares approximation. The approximation curve shows rough agreement with the experimental results. The maximum angular velocity of 714 rad/s is obtained at the steady state. From the approximation curve, the maximum angular acceleration is obtained at the initial time of motion. Also, the angular velocity is obtained at the steady state. The torque is calculated as the product of the angular acceleration and the moment of inertia of the weight and the rotor (Fig. 10(b)); peak torque of 5.36 nNm is estimated.

Fig. 11(a) shows the transient response of the micromotor with the single-crystal PMN-PT piezoelectric elements at an amplitude of 11.8 V_{p-p}. The rotor spins at lower voltages than that using PZTs. A peak torque of 2.73 nNm and a peak angular velocity of 248 rad/s are obtained from the approximation curve (Fig. 11(b)).

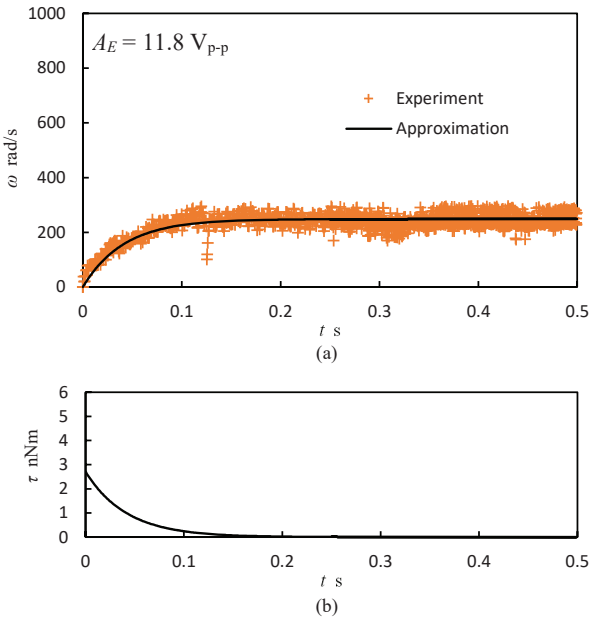

Fig. 11. Transient response of the micromotor using the stator with single crystal piezoelectric elements. (a) Experimental plots and an approximation curve obtained from the least minimum method. (b) the torque obtained from the approximated angular velocity curve.

5.3 Comparison with Existing Micromotors

Table 4 compares the proposed submillimeter-scale ultrasonic motors with similar-scale rotary electric motors. Electrostatic and electromagnetic motors were fabricated by semiconductor-based bottom-up processes and were actuated on a silicon substrate. Electrostatic micromotors have been regarded as an early achievement in MEMS. The original torque generated by the electrostatic force was of piconewton meter order [10]. To address the extremely small torque, a harmonic (wobble) drive that reduces the angular velocity and amplifies the torque was presented, achieving nano-newton meter order [9]. Miniaturization of rotary electromagnetic motors also was studied with semiconductor-based processes. An advantage of using electromagnetic force was the low voltage sufficient to drive, although the motor used a high current. A reluctance motor with a Ni-Fe-core rotor succeeded in generating a torque of 3.3 nNm [29]. In either design, the stator has dimensions with millimeter-order diameter and a thickness of tens of micrometer-order, whereas the rotor diameter is of submillimeter scale.

Piezoelectric ultrasonic motors are fabricated using a top-down process that can produce miniaturized parts

Table 4: Comparison between submillimeter-scale electric motors

Paper	Principle	Rotor dia. mm	Stator Vol. mm^3	Angular vel. rad/s	Torque nNm	Voltage V or V_{p-p}
Fan *et al.* [8]	Electrostatic	0.12	-	52.4	-	350
Jacobsen *et al.* [9]	Electrostatic	0.546	-	73.3	15	300
Ahn *et al.* [29]	Electromagnetic	0.5	-	52.4	3.3	1
Watson *et al.* [18]	Piezoelectric	1	0.080	830	47	20
Proposed (PZT)	Piezoelectric	0.15	0.032	714	5.4	44.8
Proposed (PMN-PT)	Piezoelectric	0.15	0.032	248	2.7	11.8

by micro-machining. The submillimeter-scale ultrasonic motors show much higher torque than the original torque of the silicon-based micromotors. The greatest torque has been achieved using an ultrasonic motor with a coil-shaped stator fabricated using a helical cut of laser machining [18]. The torque was amplified by the magnetic force-based preload mechanism, but a magnet of larger than 10 mm was not discussed. In terms of volume, the proposed submillimeter-scale ultrasonic motors are the smallest, although development of their performance is still progressing.

6 Conclusion

This study has demonstrated the feasibility of submillimeter-scale ultrasonic motors by building such a prototype and conducting a demonstration with it. A stator with volume of only 0.032 mm^3 is the smallest ultrasonic motor reported to date. The knowledge applied throughout this study provides deep insight into miniaturization problems that are encountered in diverse fields.

The torque obtained during the experiments is similar to or greater than that obtained for similar-sized micromotors using other principles such as electrostatics and electromagnetics. To improve the motor performance, design optimization is necessary. An important parameter is the preloading between the stator and rotor, as with ordinary-sized ultrasonic motors that enhance the torque by the preload. The fabrication methodology must be considered with the optimal design together. Although slight fabrication errors remain, improving the fabrication quality reduces the errors and improves motor performance. In the frequency response of the admittance,

the stator with 15-mode piezoelectric elements did not show good results, but we believe that this stator still has high potential. We continue the study to bring out its inherent potential. Improvement of the submillimeter-scale ultrasonic motor is of great interest in helping with new approaches and novel examination of the physical phenomena related to these micromotors, eventually overcoming the current limitations hindering micromachine development.

APPENDIX

We introduce the scale of the resonant resistance and the quality factor of the stator, the size of which changes with keeping the ratio of height, width, and depth, i.e., the shape parameters are held constant while the size changes. The scale of the micro ultrasonic motors was studied [30], but the resonant resistance and quality factors were not discussed. In [30], the stators employ a metallic cube with a side length of 2 mm, 1 mm, and 0.5 mm. Using the length parameter l, they are defined as l = 2 mm, 1 mm, and 0.5 mm. The dimensions of the piezoelectric elements and the metallic cube depend on the length parameter, while the ratio among those dimensions and material properties are constant. The hole diameters are 70% of the side length: 1.4 mm at l = 2 mm, 0.7 mm at l = 1 mm, and 0.35 mm at l = 0.5 mm. Four piezoelectric elements are bonded to four side faces of the stator using a conductive epoxy adhesive. The size of those piezoelectric elements also changes with the length parameter; the dimensions have 1.6 mm × 2 mm × 0.6 mm, 0.8 mm × 1 mm × 0.3 mm, and 0.4 mm × 0.5 mm × 0.15 mm for the stators l = 2 mm , 1 mm, and 0.5 mm, respectively.

Fig. 12 shows the scales of the resonant resistance R and the quality factor Q_m of the stator evaluated by the impedance analyzer. The resonant resistance R increases with miniaturization (Fig. 12(a)). The relationship between resonant resistance and length is roughly inversely proportional. As the size reduces, the quality factor Q_m decreases (Fig. 12(b)) because the product of ω_r and C scales as l^0 in (4). Hence, the resulting behavior of Q_m is the same as the inverse of R. The behavior of R and Q_m comes from the increase in the damping factor at high frequency.

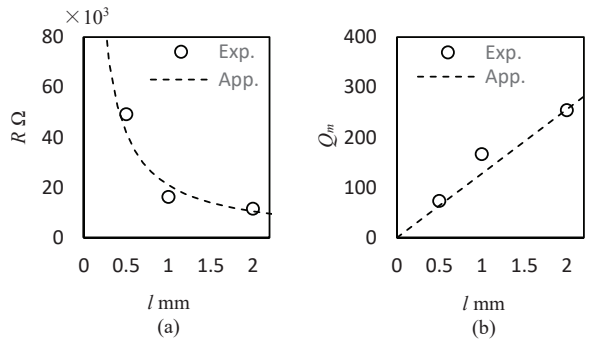

Fig. 12. Scaling of the parameters of micro-ultrasonic motors: (a) the resonant resistance and (b) the quality factor. In (a) and (b), the dotted lines are approximation curves of $R \propto l^{-1}$ and $Q_m \propto l^1$, respectively.

Acknowledgment

This work was supported by the Japan Society for the Promotion of Science (No. 19H02110) and the JST FOREST Program, Grant Number JPMJFR212G.

References

[1] H. Ishihara, F. Arai, T. Fukuda, Micro mechatronics and micro actuators, IEEE/ASME Transactions on Mechatronics 1 (1) (1996) 68–79. doi:10.1109/3516.491411.

[2] D. K.-C. Liu, J. Friend, L. Yeo, A brief review of actuation at the micro-scale using electrostatics, electromagnetics and piezoelectric ultrasonics, Acoustical Science and Technology 31 (2) (2010) 115–123. doi:10.1250/ast.31.115.

[3] T. Mashimo, S. Izuhara, Review: Recent advances in micromotors, IEEE Access 8 (2020) 213489–213501. doi:10.1109/ACCESS.2020.3041457.

[4] A. Inoue, B. Shen, A. Takeuchi, Developments and applications of bulk glassy alloys in late transition metal base system, MATERIALS TRANSACTIONS 47 (5) (2006) 1275–1285. doi:10.2320/matertrans.47.1275.

[5] T. Wang, C. Lancée, R. Beurskens, J. Meijer, B. Knapen, A. F. van der Steen, G. van Soest, Development of a high-speed synchronous micro motor and its application in intravascular imaging, Sensors and Actuators A: Physical 218 (2014) 60–68. doi:https://doi.org/10.1016/j.sna.2014.07.020.

[6] W. Trimmer, Microrobots and micromechanical systems, Sensors and Actuators 19 (3) (1989) 267–287. doi:https://doi.org/10.1016/0250-6874(89)87079-9.

[7] K. Dermitzakis, J. P. Carbajal, J. H. Marden, Scaling laws in robotics, Procedia Computer Science 7 (2011) 250–252.

[8] L.-S. Fan, Y.-C. Tai, R. S. Muller, Ic-processed electrostatic micromotors, Sensors and Actuators 20 (1) (1989) 41–47.

[9] S. Jacobsen, R. Price, J. Wood, T. Rytting, M. Rafaelof, The wobble motor: design, fabrication and testing of an eccentric-motion electrostatic microactuator, in: Proceedings, 1989 International Conference on Robotics and Automation, 1989, pp. 1536–1546 vol.3. doi:10.1109/ROBOT.1989.100197.

[10] M. Mehregany, Y.-C. Tai, Surface micromachined mechanisms and micromotors, Journal of Micromechanics and Microengineering 1 (2) (1991) 73. doi:10.1088/0960-1317/1/2/001.

[11] T. Morita, Miniature piezoelectric motors, Sensors and Actuators A: Physical 103 (3) (2003) 291–300. doi:https://doi.org/10.1016/S0924-4247(02)00405-3.

[12] B. Watson, J. Friend, L. Yeo, Piezoelectric ultrasonic micro/milli-scale actuators, Sensors and Actuators A: Physical 152 (2) (2009) 219–233. doi:https://doi.org/10.1016/j.sna.2009.04.001.

[13] X. Gao, J. Yang, J. Wu, X. Xin, Z. Li, X. Yuan, X. Shen, S. Dong, Piezoelectric actuators and motors: Materials, designs, and applications, Advanced Materials Technologies 5 (1) 1900716. doi:https://doi.org/10.1002/admt.201900716.

[14] T. Morita, M. K. Kurosawa, T. Higuchi, A cylindrical shaped micro ultrasonic motor utilizing pzt thin film (1.4 mm in diameter and 5.0 mm long stator transducer), Sensors and Actuators A: Physical 83 (1) (2000) 225–230. doi:https://doi.org/10.1016/S0924-4247(99)00388-X.

[15] S. Dong, S. Lim, K. Lee, J. Zhang, L. Lim, K. Uchino, Piezoelectric ultrasonic micromotor with 1.5 mm diameter, IEEE Transactions on Ultrasonics, Ferroelectrics, and Frequency Control 50 (4) (2003) 361–367. doi:10.1109/TUFFC.2003.1197958.

[16] T. Kanda, A. Makino, T. Ono, K. Suzumori, T. Morita, M. K. Kurosawa, A micro ultrasonic motor using a micro-machined cylindrical bulk pzt transducer, Sensors and Actuators A: Physical 127 (1) (2006) 131–138. doi:https://doi.org/10.1016/j.sna.2005.10.056.

[17] B. Watson, J. Friend, L. Yeo, Piezoelectric ultrasonic resonant motor with stator diameter less than 250 µm: the proteus motor, Journal of Micromechanics and Microengineering 19 (2) (2009) 022001. doi:10.1088/0960-1317/19/2/022001.

[18] B. Watson, J. Friend, L. Yeo, M. Sitti, Piezoelectric ultrasonic resonant micromotor with a volume of less than 1 mm3 for use in medical microbots, in: 2009 IEEE International Conference on Robotics and Automation, 2009, pp. 2225–2230. doi:10.1109/ROBOT.2009.5152400.

[19] L. Yan, H. Lan, Z. Jiao, C.-Y. Chen, I.-M. Chen, Compact piezoelectric micromotor with a single bulk lead zirconate titanate stator, Applied Physics Letters 102 (13) (2013) 134106. doi:10.1063/1.4799353.

[20] T. Mashimo, Micro ultrasonic motor using a one cubic millimeter stator, Sensors and Actuators A: Physical 213 (2014) 102–107. doi:https://doi.org/10.1016/j.sna.2014.03.018.

[21] E. T. K. Chiang, T. Mashimo, Comparison study of bending and three-wave vibration modes for micro ultrasonic motors, Sensors and Actuators A: Physical 329 (2021) 112801. doi:https://doi.org/10.1016/j.sna.2021.112801.

[22] T. Mashimo, Y. Oba, Performance improvement of micro-ultrasonic motors using the thickness shear mode piezoelectric elements, Sensors and Actuators A: Physical 335 (2022) 113347. doi:https://doi.org/10.1016/j.sna.2021.113347.

[23] K. E. Drexler, Nanosystems: Molecular Machinery, Manufacturing, and Computation, John Wiley Sons, Inc., USA, 1992.

[24] Japan Electronics and Information Technology Industries Association (JEITA), Electrical test methods for piezoelectric ceramic vibrators, standardjapan electronics and information technology industries association (JEITA EM-4501) Edition (2006).

[25] P. Hareesh, D. L. DeVoe, Miniature bulk PZT traveling wave ultrasonic motors for low-speed high-torque rotary actuation, Journal of Microelectromechanical Systems 27 (3) (2018) 547–554. doi:10.1109/JMEMS.2018.2823980.

[26] W. Zhou, J. He, L. Ran, L. Chen, L. Zhan, Q. Chen, H. Yu, B. Peng, A piezoelectric microultrasonic motor with high q and good mode match, IEEE/ASME Transactions on Mechatronics 26 (4) (2021) 1773–1781. doi:10.1109/TMECH.2021.3067774.

[27] K. Echizenya, K. Nakamura, K. Mizuno, PMN-PT and PIN-PMN-PT single crystals grown by continuous-feeding bridgman method, Journal of Crystal Growth 531 (2020) 125364. doi:https://doi.org/10.1016/j.jcrysgro.2019.125364.

[28] T. Malysh, Poling of PZT ceramics, Ph.D. thesis, Technical university of Liberec (2012).

[29] C. Ahn, Y. Kim, M. Allen, A planar variable reluctance magnetic micromotor with fully integrated stator and coils, Journal of Microelectromechanical Systems 2 (4) (1993) 165–173. doi:10.1109/84.273093.

[30] T. Mashimo, Scaling of piezoelectric ultrasonic motors at submillimeter range, IEEE/ASME Transactions on Mechatronics 22 (3) (2017) 1238–1246. doi:doi: 10.1109/tmech.2017.2691805.